

1 **Direct Measurements of the Convective Recycling of the Upper Troposphere**

2
3 Timothy H. Bertram¹, Anne E. Perring¹, Paul J. Wooldridge¹, Ronald C. Cohen^{1,2}

4
5 ¹*Department of Chemistry; University of California, Berkeley*

6 ²*Department of Earth and Planetary Science; University of California, Berkeley*

7
8 John Crounse³, Alan Kwan^{3,4}, Paul O. Wennberg^{3,4}, Eric Schauer⁵, Jack Dibb⁵, Melody
9 Avery⁶, Glen Sachse⁶, Stephanie A. Vay⁶, James H. Crawford⁶, Cameron McNaughton⁷,
10 Antony Clarke⁷, Henry Fuelberg⁸, Greg Huey⁹, William H. Brune¹⁰, Donald R. Blake¹¹,
11 Hanwant R. Singh¹², Rick Shetter¹³, Brian G. Heikes¹⁴ and Alan Fried¹⁵

12
13 ³Division of Geological and Planetary Sciences; California Institute of Technology

14 ⁴Environmental Science and Engineering; California Institute of Technology

15 ⁵Institute for the Study of Earth, Oceans, and Space; University of New Hampshire

16 ⁶NASA Langley Research Center, Hampton, VA

17 ⁷School of Ocean and Earth Science Technology; University of Hawaii, Manoa

18 ⁸Department of Meteorology; Florida State University

19 ⁹School of Earth and Atmospheric Sciences; Georgia Institute of Technology

20 ¹⁰Department of Meteorology; Pennsylvania State University

21 ¹¹Department of Chemistry; University of California, Irvine

22 ¹²NASA Ames Research Center; Moffett Field, CA

23 ¹³National Suborbital Education and Research Center; University of North Dakota

24 ¹⁴Graduate School of Oceanography; University of Rhode Island

25 ¹⁵The National Center for Atmospheric Research; Boulder, CO

1 **Abstract**

2 We present a statistical representation of the aggregate effects of deep convection on the
3 chemistry and dynamics of the Upper Troposphere (UT) based on direct aircraft
4 observations of the chemical composition of the continental UT during summer. These
5 measurements provide new and unique constraints on the chemistry occurring downwind
6 of convection and the rate at which air in the UT is recycled, previously only the province
7 of model analyses. These direct measures of atmospheric rates present a challenge to our
8 thinking about the processes governing UT ozone and its impact on climate.

1 Deep convection represents a highly efficient transport mechanism for the vertical
2 redistribution of air from near the Earth's surface (0-2 km) to the Upper Troposphere
3 (UT) (6-12 km) (1-5). Typical convective storms have spatial scales of tens of kilometers
4 and vertical velocities as large as 15 m sec^{-1} (6), while supercell and multicell storms can
5 have vertical velocities as large as 50 m sec^{-1} during their initial phases (7), making their
6 local influence in the UT extremely strong. The rapid upward flow is balanced by much
7 slower descending flow that occurs over a larger spatial scale (8). Convection is also
8 associated with lightning which dramatically enhances NO_x ($\text{NO}_x \equiv \text{NO} + \text{NO}_2$) in the UT
9 (9, 10). The source strength and spatial distribution of lightning NO_x emissions is not
10 well known, with estimates ranging from 2-20 Tg(N) yr^{-1} for the global average (11),
11 compared to 25 Tg(N) yr^{-1} from fossil fuel combustion (12). Although there have been a
12 number of case studies of the chemical effects of individual storms (6), studies of the
13 aggregate effects of convection on the chemical composition and radiative forcing of the
14 UT have been the province of modeling and theory (13) due to the absence of
15 measurements that provide an unambiguous link between an observable property and the
16 ensemble of convective events. Here we describe measurements that provide this link.

17

18 The chemical and radiative consequences of convection and lightning are known to be
19 large (2, 3, 14). Upper tropospheric O_3 , either transported directly from the boundary
20 layer via convection or formed *in situ* following detrainment of convectively lofted O_3
21 precursors (NO_x , HO_y and hydrocarbons) in the outflow region, directly impacts climate
22 through a positive radiative forcing of $0.4\text{-}0.78 \text{ W m}^{-2}$ as a global annual tropospheric
23 average (14). Additionally, deep convection accounts for a significant fraction of the net

1 flux of moisture from near the Earth's surface to the UT during the summer months.
2 Thus, understanding the rate at which the UT is turned over by convection has important
3 implications on the spatial and temporal distribution of clouds, and their associated
4 effects on the Earth's radiative budget.

5
6 In this study we describe a method for calculating the time air spends in the upper
7 troposphere following convection from *in situ* measurements of the chemical composition
8 of the UT and discuss the chemistry occurring in the outflow region as a function of time
9 since convection. We use measurements of NO₂ (15, 16) (NO_x is calculated from NO₂,
10 O₃, HO₂ and photolysis rates), HNO₃ (17) (*Wennberg CIMS inst. ref.*), OH and HO₂ (18),
11 O₃ (19), aerosol number density (*Clarke inst. ref.*), photolysis rates (20), CO (21) and
12 CO₂ (22) obtained during the Intercontinental Chemical Transport Experiment – North
13 America (INTEX-NA) aboard the NASA DC-8 over the continental United States (23).
14 Measurements were made at altitudes between the surface and 12.5 km, over a wide area
15 of the US and Canada, west of 40° W and between 30 and 50° N. There were a large
16 number of vertical profiles allowing a reasonably unbiased statistical sampling of air over
17 Eastern North America during July and August of 2004.

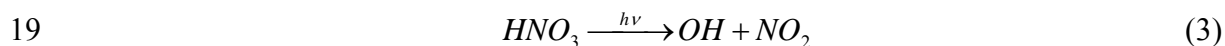
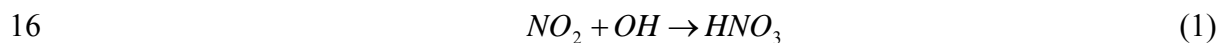
18
19 In this study we use the deviation of the observed NO_x to HNO₃ ratio from steady-state as
20 an indicator of convective influence. The NO_x to HNO₃ ratio is reinitialized in moist
21 convection as a result of preferential wet scavenging of HNO₃ relative to NO_x (i.e. the
22 Henry's Law Constant for HNO₃ is 10⁸ larger than for NO_x) (24). Further, lightning
23 initiated NO_x production, often coincident with convection, dramatically enhances NO_x in

1 the outflow region. The coupling of these processes makes the NO_x to HNO_3 ratio an
 2 effective indicator of convective influence, where $\text{NO}_x/\text{HNO}_3 \gg 1$ is indicative of recent
 3 cloud outflow (25, 26). In the days following convection, the ratio decays toward steady-
 4 state providing a chemical clock that marks the time an air-mass has spent in the UT
 5 following convection. The time evolution of NO_x/HNO_3 following convection depends
 6 largely on the partitioning of NO_x (between NO and NO_2), the concentration of OH and
 7 the solar flux, all of which were measured during these experiments. Given these
 8 constraints, it is possible to create a mapping from NO_x/HNO_3 to the time that has passed
 9 since convective influence from a relatively simple system of kinetic equations.

10

11 **Reactive Nitrogen Partitioning in the UT**

12 The only significant chemical sinks of UT NO_x are reaction with OH to produce HNO_3
 13 (Equation 1) and nighttime loss through $\text{NO}_3/\text{N}_2\text{O}_5$ (Equation 2a-b). NO_x is regenerated
 14 by nitric acid photolysis (and subsequent NO_3 photolysis to NO_2) and reaction of OH
 15 with HNO_3 (Equations 3 and 4).



21 Including the altitude dependent rain-out rate for HNO_3 ($k_{\text{rain-out}}$) as derived by Giorgi and
 22 Chameides (27), the expected steady-state NO_x/HNO_3 is:

23

$$1 \quad \left(\frac{[NO_x]}{[HNO_3]} \right)_{Steady-State} = \frac{J_{HNO_3} + k_{HNO_3+OH} [OH] + k_{HNO_3 \text{ rainout}}}{\left(k_{NO_2+OH} [OH] + 2k_{N_2O_5+H_2O} \frac{[N_2O_5]}{[NO_2]} \right) x \left(\frac{[NO_2]}{[NO_x]} \right)} \quad (3)$$

2
3 Our observations, throughout the continental UT during the summer of 2004, show the
4 NO_x to HNO₃ ratio to be largely out of steady-state at pressure altitudes greater than 6 km
5 (c.f. Figure 2). The deviation from steady-state climbs rapidly as a function of altitude
6 before reaching a maximum at 10 km. Previous observations of NO_x and HNO₃ (either
7 measured directly or calculated from observations of NO_x, PAN and NO_y) have shown
8 the NO_x/HNO₃ ratio to be significantly larger than the steady-state prediction in the UT
9 (25, 26, 28-32). This has been shown to be primarily a result of convection and lightning
10 reinitializing the system before steady-state is achieved (25, 26). Although a series of
11 other hypotheses have been put forth (30-32), we (like Jaegle et al.) find no evidence for
12 a mechanism other than convection responsible for holding NO_x/HNO₃ out of steady-
13 state in the UT.

14

15 **Chemical Signatures of Convection**

16 Figure 3 depicts one of many convectively influenced air-masses sampled in the UT
17 during INTEX-NA. Three distinct convective events (40–80 km wide) are identified by
18 enhancements in NO_x/HNO₃ in Figure 3a. Coincident enhancements are present in SO₂,
19 an indicator of a recent boundary layer source for this air, and Ultra-fine Cloud
20 Condensation Nuclei (UCN) ($3 \leq D_p \leq 10$ nm), an indicator of cloud detrainment (Figure
21 3b) (33, 34). Sharp decreases in CO₂ also indicate the convective lofting of boundary
22 layer air depleted in CO₂, a result of seasonal photosynthetic activity in the biosphere

1 (Figure 3c) (34). Enhancements in Carbon Monoxide, Formaldehyde and other
2 hydrocarbons, relative to the surrounding UT air, were also observed in these plumes.
3 Backward air trajectories, initialized along the flight track, coupled to the spatial and
4 temporal distribution of cloud-ground lightning strikes, indicate that the sampled air-mass
5 was recently influenced by lightning approximately one day prior to DC-8 sampling (c.f.
6 Figure 3 bottom panel) (35). Such features with high NO_x/HNO_3 were observed
7 throughout the UT during INTEX-NA.

8

9 To assess the extent to which the UT is influenced by convection and describe the
10 chemical evolution of convective outflow, we use a constrained time-dependent photo-
11 chemical box model to create a mapping of the observed NO_x/HNO_3 to the time since the
12 ratio was last reinitialized. The model is initialized with observations from the INTEX-
13 NA field campaign and run at 1km vertical intervals from 6 to 12 km. A description of
14 the model is presented in the supplemental information included with this article. The
15 derived timing indicator for the convectively influenced air sampled on 11 August 2006
16 is shown in Figure 3d. The properties of the ensemble of measurements obtained in the
17 UT during summer 2004 are shown in Figures 4-6.

18

19 The aerosol size distribution provides an independent indicator of air recently detrained
20 from clouds. Cloud processed air is depleted of aerosol surface area permitting new
21 particle formation in the outflow region (33, 34). Figure 4a depicts the fraction of
22 condensation nuclei found in the 3-10 nm bin as a function of time since convective
23 influence. The fraction of particles in this ultra-fine mode is largest during the first few

1 days confirming that the NO_x to HNO_3 ratio, and the timing indicator derived from it, is
2 reinitialized in the UT by cloud processing. Strong enhancements in $\text{CH}_3\text{OOH}/\text{H}_2\text{O}_2$ (not
3 shown), also an indicator of recent cloud processing (36, 37), were observed during the
4 first two days after cloud processing.

5
6 As expected, both elevated NO_x and suppressed HNO_3 are observed at short times (c.f.
7 Figure 4b-c). Enhancements in NO_x during the first few days is indicative of convection
8 of boundary layer and/or lightning NO_x (38, 39). The suppression of HNO_3 at short times
9 is clear indication of HNO_3 scavenging during convection. Figure 4d confirms that
10 reactive nitrogen ($\text{NO}_y \equiv \text{NO}_x + \Sigma\text{PNs} + \text{HNO}_3$), 80% of which is either NO_x or HNO_3 , is
11 conserved during the chemical processing following convection, a fact which provides
12 further support for the use of NO_x/HNO_3 as a marker representing time since convection.
13 Time-dependent model results, initialized at 10 km and 12PM with $[\text{NO}_x]_i = 800$ pptv,
14 $[\text{O}_3]_i = 65$ ppbv and $[\text{CO}]_i = 105$ ppbv are shown with solid black lines for NO_x , HNO_3
15 and NO_y .

16

17 **Chemical Processing in Convective Outflow**

18 Using the observed NO_x to HNO_3 ratio and the timing indicator generated from it, we can
19 remap the ensemble of observations made throughout the UT onto the coordinate of time
20 since convection. This allows us to assess the chemical and dynamical processes
21 occurring following convection, without attempting a Lagrangian convection study. In
22 this analysis we concentrate on the time evolution of CO and O_3 , however parallel

1 analysis could be conducted on various other species measured in this study (e.g.
2 Acetone, Methanol and H₂CO among others).

3

4 The time evolution of CO following convective injection into the UT is set by the
5 abundance of OH and the rate at which the convective plume entrains air from the
6 background UT. Due to the direct dependence of the chemical clock on HO_x, we
7 constrained both OH and HO₂ to the observations as a function of NO_x and pressure in
8 the time-dependent model used to generate time. As a result, we can iterate the model to
9 determine the proper dilution rate of the convective plume by matching the modeled and
10 observed time evolution of CO following convection. Using this approach for a series of
11 long lived species (e.g. CO, CH₄, CH₃OH and others), we calculate an average dilution
12 rate of $0.05 \pm 0.02 \text{ day}^{-1}$ following convective injection into the UT. This is significantly
13 slower than the mixing rate determined by Price et al. ($0.01 \pm 0.004 \text{ hr}^{-1}$) for transpacific
14 long range transport (40). Figure 5a depicts the observed time evolution of CO following
15 convection, along with the modeled decay in CO stemming from both chemical loss and
16 entrainment of background UT air suppressed in CO relative to the convective plume.
17 The shaded region depicts the 1st – 3rd quartiles of the observations and represents the
18 atmospheric variance in the chemical composition of convective outflow. Chemical loss
19 in our model represents over 60% of the observed loss in CO during the first five days
20 following injection.

21

22 The measured abundance of UT O₃ as a function of time since convection in the UT is
23 shown in Figure 5b, where the median (-o-) mixing ratio within 8 hour bins of time are

1 shown in red, the shaded region represents the 1st and 3rd quartiles. We find that on
2 average, convectively lofted air masses contain less O₃ than the background UT. This
3 result is consistent with the observed vertical gradient in O₃ over the continental US, with
4 lower O₃ in the Planetary Boundary Layer (PBL) than above.

5

6 The rate of change of the observed O₃ mixing ratio as a function of time since convection
7 is shown in Figure 5b. For comparison, results from a model initialized with
8 observations characteristic of fresh convective outflow is shown in grey. Rapid changes
9 in the O₃ mixing ratio are observed during the first two days following detrainment, with
10 the observed O₃ 15 ppbv above the initial value by the end of day two. The observed rate
11 of increase slows exponentially with an asymptote at long time approaching zero and the
12 O₃ mixing ratio approaching a constant value of 85 ppbv. This is a surprising result, as
13 our model of the O₃ rate of change never approaches zero, but continues to predict a net
14 increase of 3 ppbv O₃ day⁻¹ at the end of day five.

15

16 Net Δ_{Ozone} of 0 ppbv day⁻¹ could be achieved if the air parcel: i.) subsided to where H₂O
17 abundances are large enough to provide a sink of O₃ through O¹D that balanced
18 production from NO+HO₂ (~6 km), ii.) entrained air containing lower O₃ mixing ratios or
19 iii.) contained additional O₃ loss terms beyond NO_x, HO_x, H₂O (via O¹D removal). To
20 match the deviation between the model and measurement, we would require an additional
21 2-3 ppbv day⁻¹ of chemical ozone loss. In order for mixing to explain the deviation, air of
22 lower O₃ would need to be mixed into the air parcel. As shown in Figure 5b, the only air
23 in the UT containing significantly less O₃ is that pumped directly from the PBL. While

1 mixing fresh and aged outflow could help to explain the discrepancy in O₃, it is
2 inconsistent with the observed decay in CO at long time (2-5 days). The source of this O₃
3 loss is an open puzzle.

4

5 **Constraints on the Convective Turnover Rate of the UT**

6 The convective turnover rate of the upper troposphere is critical for accurately describing
7 NO_x, HO_x and O₃ chemistry in the UT (41). However, at present there is a paucity of
8 observation based constraints available (either meteorological or chemical) to test the
9 aggregate effects of convection in the current generation of global climate models. In
10 this analysis we use ensemble statistics of the UT, generated from the aforementioned *in*
11 *situ* observations, to provide a direct observable constraint for the mean convective
12 turnover rate of the continental UT during summer. To determine the convective
13 turnover rate of the UT from the observations presented here, both the extent to which the
14 UT is influenced by convection and the fraction of BL air in the convectively influenced
15 air masses must be known with high confidence.

16

17 To determine the fraction of BL air contained in a convective plume, we use observations
18 of insoluble long-lived species (e.g. CO, CH₄, CO₂, CH₃OH and C₂H₆) made throughout
19 the INTEX-NA campaign over the continent. Fresh convective outflow ($t < 12$ hours) is
20 identified using our timing indicator derived from the NO_x to HNO₃ ratio. Assuming that
21 we conducted a statistically unbiased sampling of both the boundary layer and free
22 troposphere during INTEX-NA, we can calculate the fraction of BL air present in fresh
23 convection (f) through the following equation:

1

$$2 \quad [X]_{UT(t=0)} = f [X]_{BL} + (1-f) [X]_{UT} \quad (4)$$

3

4 where $[X]_{UT(t=0)}$ is the mean mixing ratio of species X in fresh convective outflow (as
 5 identified using our timing indicator), $[X]_{UT}$ is the mean mixing ratio of species X in the
 6 UT (7.5-11.5 km) and $[X]_{BL}$ is the mean mixing ratio of species X in the BL (0-1.5 km).
 7 Using observations of CO, CH₄, CO₂, CH₃OH and C₂H₆ we calculate the fraction of BL
 8 air in fresh convection to be 0.18, 0.05, 0.10, 0.26 and 0.26, respectively. Note that the
 9 calculation for CH₄ (and CO₂ to a lesser extent) is the least reliable because of the small
 10 differences between large numbers. Omitting CH₄ we calculate a mean value for the
 11 fraction of BL air in convective outflow of 0.20 ± 0.1 . This is in agreement with the
 12 modeling studies of Mullendore et al., who calculate the fraction of BL air present in the
 13 convective outflow region of a supercell storm to be between 0.2 and 0.5 (7) .

14

15 Figure 6a shows the normalized frequency distribution of the observed time since
 16 convection based on the ratio of NO_x to HNO₃. The data are sorted into 1km bins
 17 throughout the 7.5 to 11.5 km region. We find that 54% of the air sampled between 7.5
 18 and 11.5km had been influenced by convection during the past two days. The convective
 19 outflow was strongest between 9.5 and 10.5 km, where the fraction of sampled air that is
 20 less than two days old exceeds 69%. The vertical distribution presented here is consistent
 21 with previous observations and model analyses of convective outflow from individual
 22 storms (4, 42). The shift toward longer times between 10.5 and 11.5 km suggests that
 23 either convective cloud tops on average do not extend higher than 10.5 km over the mid-

1 latitude during the summer (*ref. for mid-latitude cloud top heights?*) or that transport of
2 stratospheric air, rich in HNO₃, contributes to keeping the NO_x to HNO₃ ratio low at
3 altitudes greater than 10.5 km (43).

4

5 These results are consistent with the purely meteorological assessment of convective
6 influence of Fuelberg et al. (35). In their analysis, 10-day back trajectories to National
7 Weather Service Global Forecast System (GFS) derived convection and National
8 Lightning Detection Network (NLDN) measured lightning strikes are used to assess the
9 fraction of time that the DC-8 sampled either convection or lightning influenced air.
10 Using the GFS statistics, Fuelberg et al. calculate that 63% of the sampled air on INTEX-
11 NA had encountered convection and ~57% had been influenced by lightning during the
12 past 2 days. In Fuelberg et al., the authors determine that when considering the entire
13 INTEX-NA sampling domain (both in space and time), convection was present in 12.5%
14 of the grid points. This is substantially smaller than the percent of observations within 6
15 hours of convection (21.4%), suggesting that the DC-8 had a positive bias toward
16 sampling fresh convection. This bias is reflected in the sharp drop in population between
17 day 1 and 2 as shown in Figure 6a. Correcting for this bias has little affect on our
18 assessment of the fraction of air less than 2 days old, lowering our results from 0.43,
19 0.56, 0.69 and 0.43 to 0.38, 0.50, 0.62 and 0.39 at 8, 9, 10 and 11 km respectively.

20

21 To provide constraint on the turnover rate of the UT from the ensemble statistics
22 generated from our observed time since convective influence calculation (Figure 6a), we
23 constructed a simple two dimensional box model of the UT. In this model, we represent

1 the UT as a random set of boxes moving through the INTEX-NA sampling domain. We
2 assume that it takes 4 days for any individual box to pass through the sampling region
3 and that each box has not been influenced by convection upon entering the sampling
4 window. Every six hours we: i.) represent convection by randomly reinitializing the age
5 of x% of the boxes in the sampling domain to 0 (the value of x is determined by the
6 turnover rate (varied between 5 and 20% day⁻¹) and the fraction of BL air contained in a
7 convective plume of 0.2) and ii.) dilute each box with the mean value of the adjacent 8
8 boxes at the rate of 5% day⁻¹.

9

10 Figure 6b depicts the observed normalized frequency distribution of time since
11 convective influence between 7.5 and 11.5 km (grey bars). The shape of the distribution
12 suggests that UT air sampled during INTEX-NA was largely influenced by convection,
13 and that convectively lofted plumes did not have sufficient time to either mix or age
14 within the sampling window achieved by the DC-8. Frequency distributions of time
15 since convection, in the Eastern half of the 2-D UT model analysis (where we sampled
16 most frequently) are also shown in Figure 6b. Model analyses using convective turnover
17 rates of 5, 10 and 20% day⁻¹ are shown in green (-◇-), blue (-○-) and red (-□-),
18 respectively. Assuming the DC-8 made a statistically unbiased sampling of the
19 continental UT during summer, we predict a convective turnover rate between 10-20%
20 day⁻¹. However, if we assume the DC-8 had a positive bias toward sampling fresh
21 convection (less than 6 hours) in accordance with Fuelberg et al., our observed frequency
22 distributions are consistent with a convective turnover rate closer to 10% day⁻¹.

23

1 A convective turnover rate of 10-20 % day⁻¹ corresponds to a mass flux of 1.5-3 kg m⁻²
2 sec⁻¹ of BL air transported to the UT (8-11 km). This is significantly larger than the value
3 of 1.6 kg m⁻² sec⁻¹ (5% day⁻¹, from the BL to 8–17 km) that Prather and Jacob reported
4 over the equatorial region (a region we expect to be more convectively active than the
5 continental mid-latitudes), derived from convection parameterizations in the GISS
6 general circulation model (25). However our derived flux is consistent, if not smaller than
7 the results of Allen et al., who report a cumulus mass flux of approximately 2.5 kg m⁻²
8 sec⁻¹ (from the BL to 8-11km for 20°-40° N) between July 1-7, 1991 using GEOS-1 DAS
9 (44) and Pickering et al., who report a cloud mass flux between 4 and 8 kg m⁻² sec⁻¹ for
10 June of 1985 (from the BL to the UT, 90°-105° W, 32.5°-50°N) using GCE ISCCP (45).

11

12 **Conclusions**

13 In this analysis we present a statistical representation of the aggregate effects of
14 convection on the chemistry and dynamics of the upper troposphere using *in situ*
15 measurements taken aboard the NASA DC-8 during the summer of 2004. These
16 observations provide a new and unique constraint on: i.) the extent to which convection
17 perturbs the continental UT during summer, ii.) the fraction of boundary layer air present
18 in convective outflow and iii.) the convective overturn rate of the upper troposphere, each
19 previously only the province of model analyses. In addition, the chemical clock
20 described here defines a coordinate that can be used to assess the chemistry occurring
21 down-wind of convective injection. In general we find the rates governing the convective
22 recycling of the UT to be faster and the aggregate chemical effects of convection to be

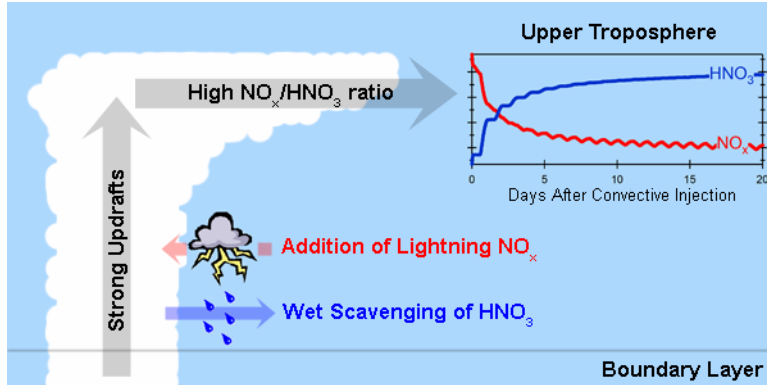
1 more widespread than most current model representations of convective influence in the
2 upper troposphere.

3

4 **Acknowledgements:**

5 The authors thank the flight and ground crews of the NASA DC-8 Aircraft and the entire
6 INTEX-NA science team for their contributions during the 2004 intensive field
7 campaign. NLDN data was provided to the INTEX science team by Vaisalia-
8 Thunderstorm. Work at U.C. Berkeley was supported by *NASA grant # ...* The INTEX-
9 NA field program was supported by the NASA-ESE TCP.

1

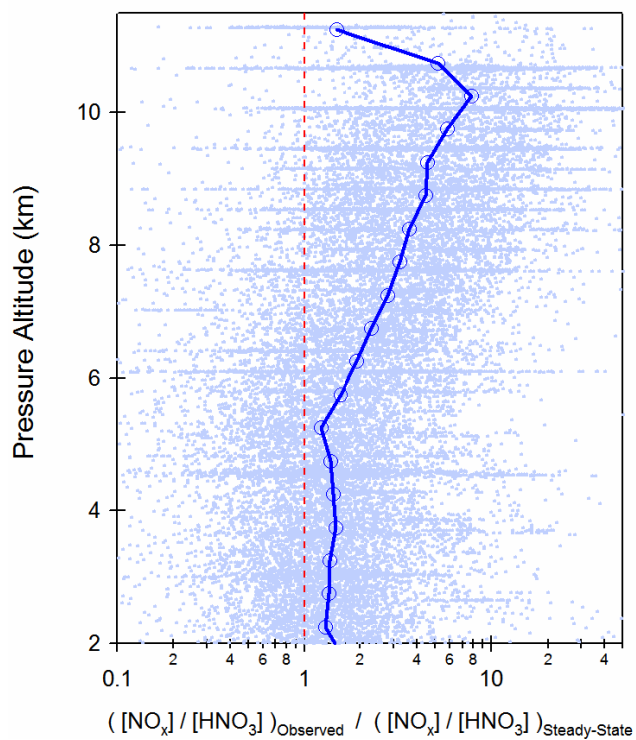


2

3

4 **Figure 1:** In moist convection, air from near the Earth's Surface is rapidly transported
 5 upwards and detrained into the Upper Troposphere. In this process, Nitric Acid (highly
 6 soluble) is efficiently scavenged, while NO_x (insoluble) remains. NO_x is dramatically
 7 elevated by concurrent lightning NO production, resulting in high NO_x to HNO₃ ratios in
 8 the convective outflow region. Following detrainment into the UT, NO_x is converted to
 9 HNO₃ by OH during the day and via NO₃/N₂O₅ at night. The chemical evolution of the
 10 NO_x/HNO₃ ratio provides a unique indicator of the time a sampled air-mass has been in
 11 the UT following convection.

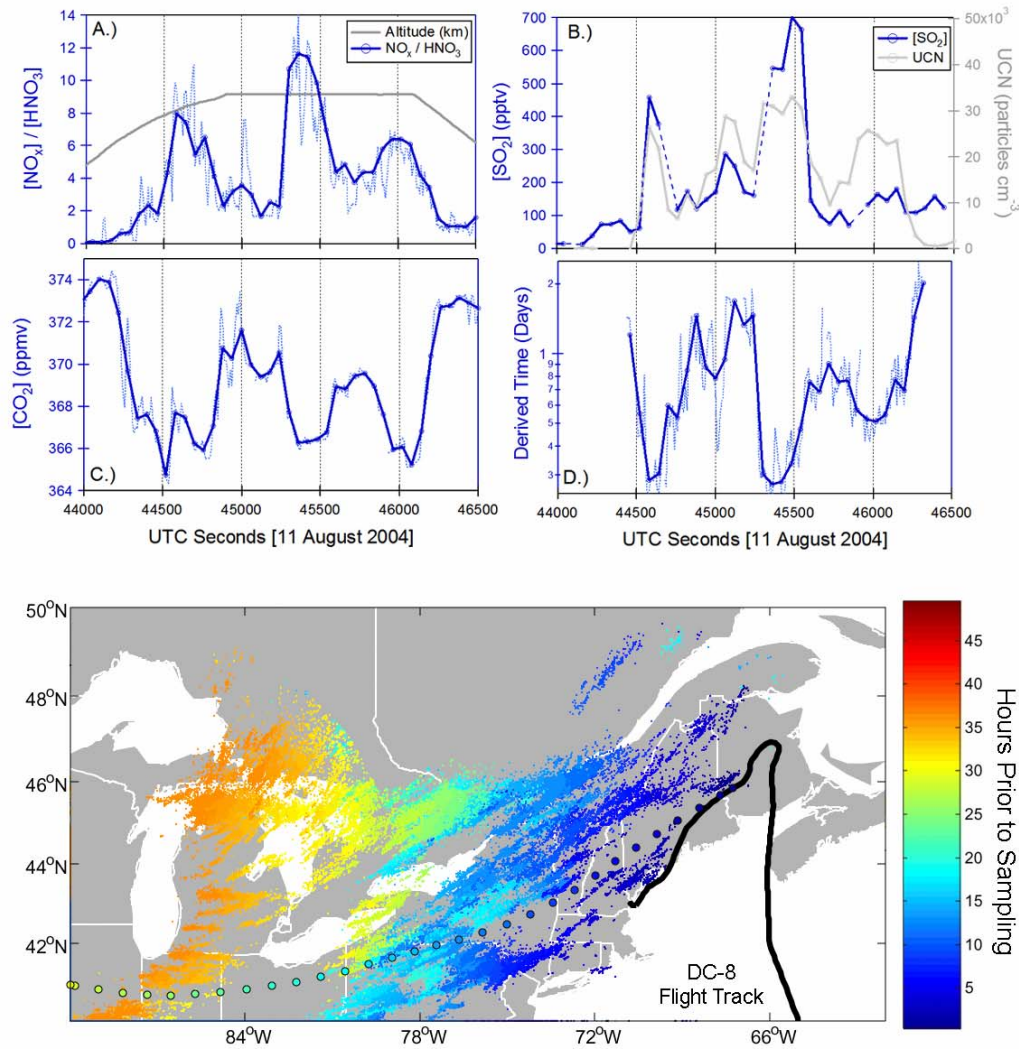
1



2

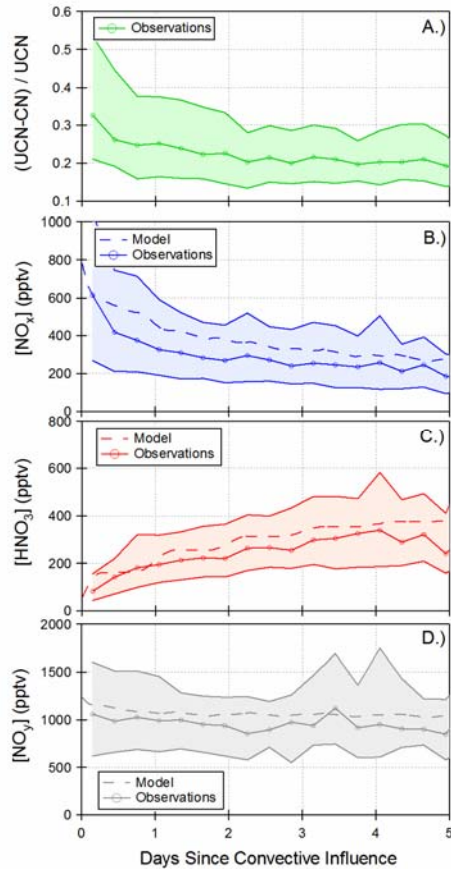
3

4 **Figure 2:** The observed deviation of the NO_x to HNO_3 ratio from steady-state as a
 5 function of altitude in the UT. The mean values within 500 m vertical bins are shown
 6 with circles (\circ). The steady-state NO_x to HNO_3 ratio was calculated from measured NO_x ,
 7 OH and J_{HNO_3} and includes the rain out parameterization of Giorgi and Chameides
 8 (1985).



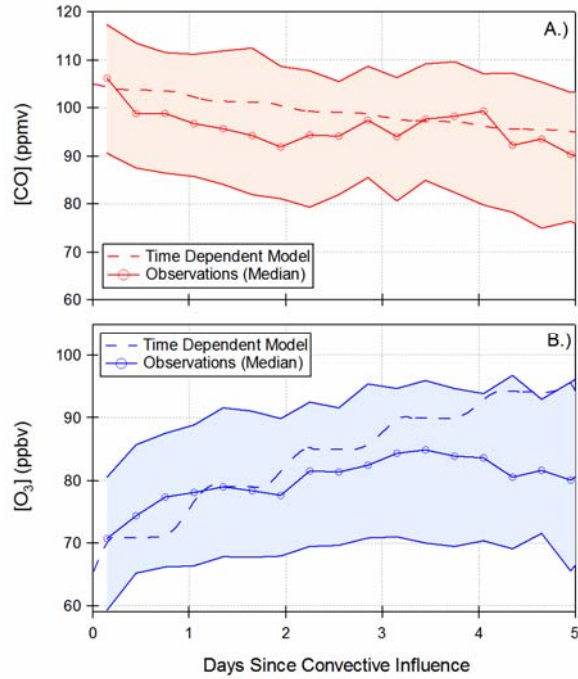
1

2 **Figure 3:** *top panel* Time series of measurements taken in the vicinity of recent
3 convective activity on 11 August 2004 between 5 and 9 km. Panel A suggests the
4 sampling of a series of fresh convective plumes, indicated by a sharp increase in the
5 NO_x/HNO_3 ratio away from steady-state. Panels B & C depict coincident enhancements
6 in SO_2 and UCN ($3\text{nm} > D_p > 10\text{nm}$) and coincident sharp drops in CO_2 , indicative of the
7 convective lofting of boundary layer air depleted in CO_2 . The derived time since the
8 sampled air-mass had been influenced by convection is shown in Panel D. *bottom panel*
9 NLDN lightning hits (small dots) on the 10th and 11th of August color-coded by time
10 (hours) prior to sampling. The DC-8 sampling location corresponding to measurements
11 shown in Figure 1 is located on the Maine – New Brunswick border [46°N 67°W]. The
12 two day back trajectory [•] (initialized at the point of the second convective plume shown
13 in Panel A) is also color-coded by time prior to DC-8 sampling (black border).



1
2
3
4
5
6
7
8

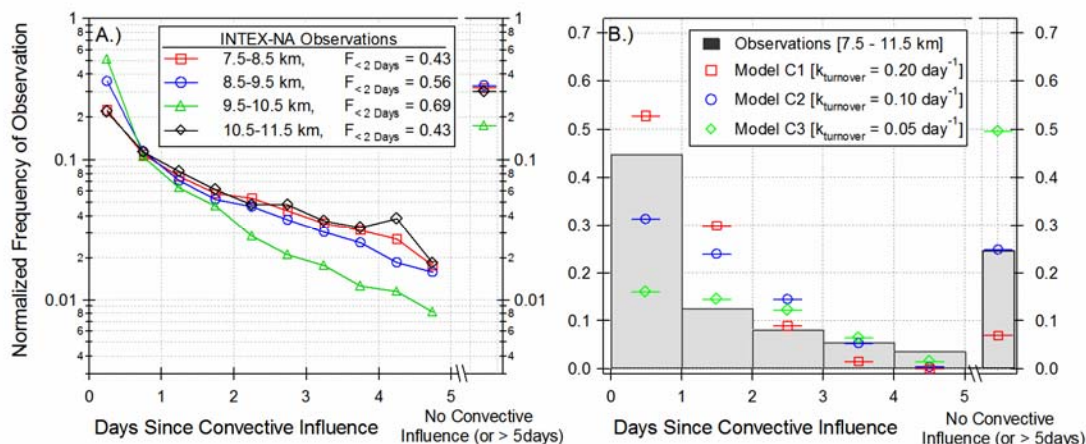
Figure 4: Observations of the fraction of ultra-fine condensation nuclei [number density of aerosol (3-10 nm) / total aerosol number density] (Panel A), NO_x (Panel B), HNO_3 (Panel C) and NO_y (Panel D) as a function of modeled time since convective influence. The median (-o-) of the observations, within 8 hour bins, is shown along with the 1st and 3rd quartiles (shaded region). Results from the time-dependent box model, initialized at 10 km and 12PM, are shown with dashed lines.



1
2
3
4
5
6

Figure 5: Observations of CO (Panel A) and Ozone (Panel B) as a function of modeled time since cloud processing in the UT. The median (-o-) of the observations, within 8 hour bins, is shown along with the 1st and 3rd quartiles (shaded region). Results from the time-dependent box model, initialized at 10 km and 12PM, are shown with dashed lines.

1



2

3

4

5

6

7

8

9

10

Figure 6: *left panel* Normalized frequency distribution in the time since convective influence, as calculated from observations of the NO_x to HNO_3 ratio made during the summer of 2004. Calculations are separated into 1 km altitude bins (ranging from 7.5-11.5 km). The fraction of air that had been influenced by convection within the past two days ($f_{<2 \text{ days}}$) is included in the figure legend. *right panel* Comparison of observed frequency distribution (7.5-11.5 km) with various modeled representations of the convective turnover rate.

References:

1. R. B. Chatfield, P. J. Crutzen, *Journal of Geophysical Research-Atmospheres* **89**, 7111 (1984).
2. R. R. Dickerson *et al.*, *Science* **235**, 460 (Jan 23, 1987).
3. K. E. Pickering, R. R. Dickerson, G. J. Huffman, J. F. Boatman, A. Schanot, *Journal of Geophysical Research-Atmospheres* **93**, 759 (Jan 20, 1988).
4. A. M. Thompson *et al.*, *Journal of Geophysical Research-Atmospheres* **99**, 18703 (Sep 20, 1994).
5. W. J. Collins, R. G. Derwent, C. E. Johnson, D. S. Stevenson, *Q.J.R. Meteorol. Soc.* **128**, 991 (2002).
6. J. E. Dye *et al.*, *Journal of Geophysical Research-Atmospheres* **105**, 10023 (Apr 27, 2000).
7. G. L. Mullendore, D. R. Durran, J. R. Holton, *Journal of Geophysical Research-Atmospheres* **110** (Mar 25, 2005).
8. S. A. Rutledge, R. A. Houze, M. I. Biggerstaff, T. Matejka, *Monthly Weather Review* **116**, 1409 (Jul, 1988).
9. H. Huntrieser, H. Schlager, C. Feigl, H. Holler, *Journal of Geophysical Research-Atmospheres* **103**, 28247 (Nov 20, 1998).
10. B. Ridley *et al.*, *Journal of Geophysical Research-Atmospheres* **109** (Sep 8, 2004).
11. “Scientific assessment of ozone depletion” (World Meteorological Organization, 1995).
12. L. Jaegle, L. Steinberger, R. V. Martin, K. Chance, *Faraday Discussions* **130**, 1 (2005).
13. J. Lelieveld, P. J. Crutzen, *Science* **264**, 1759 (Jun 17, 1994).
14. M. Gauss *et al.*, *Journal of Geophysical Research-Atmospheres* **108** (May 13, 2003).
15. J. A. Thornton, P. J. Wooldridge, R. C. Cohen, *Analytical Chemistry* **72**, 528 (Feb 1, 2000).
16. P. A. Cleary, P. J. Wooldridge, R. C. Cohen, *Applied Optics* **41**, 6950 (Nov 20, 2002).
17. R. W. Talbot *et al.*, *Geophysical Research Letters* **26**, 3057 (Oct 15, 1999).
18. I. C. Faloona *et al.*, *Journal of Atmospheric Chemistry* **47**, 139 (Feb, 2004).
19. M. A. Avery, *Submitted Journal of Oceanic and Atmospheric Technology* (2006).
20. R. E. Shetter, M. Muller, *Journal of Geophysical Research-Atmospheres* **104**, 5647 (Mar 20, 1999).
21. G. W. Sachse, G. F. Hill, L. O. Wade, M. G. Perry, *Journal of Geophysical Research* **92**, 2071 (1987).
22. S. A. Vay *et al.*, *Journal of Geophysical Research* **104**, 5663 (1999).
23. H. B. Singh, W. H. Brune, J. H. Crawford, D. J. Jacob, *Submitted Journal of Geophysical Research - Atmospheres* (2006).
24. R. Sander, R. Sander, Ed. (1999).
25. M. J. Prather, D. J. Jacob, *Geophysical Research Letters* **24**, 3189 (Dec 15, 1997).
26. L. Jaegle *et al.*, *Geophysical Research Letters* **25**, 1705 (May 15, 1998).

27. F. Giorgi, W. L. Chameides, *Journal of Geophysical Research-Atmospheres* **90**, 7872 (1985).
28. D. D. Davis *et al.*, *Journal of Geophysical Research-Atmospheres* **101**, 2111 (Jan 20, 1996).
29. D. J. Jacob *et al.*, *Journal of Geophysical Research-Atmospheres* **101**, 24235 (Oct 30, 1996).
30. R. B. Chatfield, *Geophysical Research Letters* **21**, 2705 (Dec 1, 1994).
31. A. Tabazadeh *et al.*, *Geophysical Research Letters* **25**, 4185 (Nov 15, 1998).
32. D. A. Hauglustaine, B. A. Ridley, S. Solomon, P. G. Hess, S. Madronich, *Geophysical Research Letters* **23**, 2609 (Sep 15, 1996).
33. A. D. Clarke *et al.*, *Journal of Geophysical Research-Atmospheres* **104**, 5735 (Mar 20, 1999).
34. H. Huntrieser *et al.*, *Journal of Geophysical Research-Atmospheres* **107** (Jun, 2002).
35. H. E. Fuelberg, M. J. Porter, C. M. Kiley, D. Morse, *Submitted Journal of Geophysical Research - Atmospheres* (2006).
36. D. S. Cohan, M. G. Schultz, D. J. Jacob, B. G. Heikes, D. R. Blake, *Journal of Geophysical Research-Atmospheres* **104**, 5717 (Mar 20, 1999).
37. J. A. Snow *et al.*, *Submitted Journal of Geophysical Research - Atmospheres* (2006).
38. O. R. Cooper *et al.*, *accepted Journal of Geophysical Research - Atmospheres* (2006).
39. R. C. Hudman *et al.*, *Submitted Journal of Geophysical Research - Atmospheres* (2006).
40. H. U. Price, D. A. Jaffe, O. R. Cooper, P. V. Doskey, *Journal of Geophysical Research-Atmospheres* **109** (Jul 21, 2004).
41. D. Rind, J. Lerner, *Journal of Geophysical Research-Atmospheres* **101**, 12667 (May 20, 1996).
42. K. E. Pickering, Y. S. Wang, W. K. Tao, C. Price, J. F. Muller, *Journal of Geophysical Research-Atmospheres* **103**, 31203 (Dec 20, 1998).
43. J. Dibb, E. Scheuer, R. Talbot, M. Avery, *Submitted Journal of Geophysical Research - Atmospheres* (2006).
44. D. J. Allen, R. B. Rood, A. M. Thompson, R. D. Hudson, *Journal of Geophysical Research-Atmospheres* **101**, 6871 (Mar 20, 1996).
45. K. E. Pickering *et al.*, *Geophysical Research Letters* **22**, 1089 (May 1, 1995).

1 Supplemental Online Information

2

3 1. INTEX-NA Experiment Description and Instrument Descriptions

4 The Intercontinental Chemical Transport Experiment – North America (INTEX-NA)
5 took place between 1 July and 14 August 2004. Research flights were conducted out of
6 Dryden Flight Research Center (Edwards AFB, CA), Mid-America Airfield (Mascoutah,
7 IL); and PEASE International Trade-Port (Portsmouth, NH). Figure S1 depicts the
8 vertical and horizontal extent of research flights conducted aboard the NASA DC-8
9 during INTEX-NA (*I*). DC-8 flight tracks are shown in the left panel of Figure 1 and the
10 number of samples (10 second averaging time) in 1km vertical bins are shown in the right
11 panel.

12

13 *In situ* observations relevant to this study include; NO₂, HNO₃, OH, O₃, CO, CO₂, SO₂
14 and Ultra-fine Condensation Nuclei (UCN). Table S1 describes the detection threshold,
15 uncertainty and time response for each measurement used in this analysis.

16

17 2. 0-D Time Dependent Model

18 The chemical evolution of convective outflow was modeled using a 0-D time dependent
19 model. The model was initialized with chemical conditions, altitudes and detrainment
20 times consistent with observations of fresh convection made during INTEX-NA. As time
21 propagates in the model, we calculate the production and loss of O₃, CO, NO, NO₂, NO₃,
22 N₂O₅, PAN, HO₂NO₂, HNO₃, OH, HO₂, RO₂, H₂O₂, CH₃OOH, H₂CO and C1-C6
23 Hydrocarbons for 20 days following cloud detrainment. The conversion of NO_x to HNO₃

1 in the outflow region is used as an indicator of time since convection. Figure S2 depicts
2 the results of a single run initialized at 10km with a noon detrainment time. Initial
3 conditions correspond to $[\text{NO}_x]_i = 800$ pptv, $[\text{O}_3]_i = 65$ ppbv and $[\text{CO}]_i = 105$ ppbv. Rapid
4 conversion of NO_x to HNO_3 is observed during the first few days as the system
5 approaches steady-state. In this analysis we assume: i.) HNO_3 and H_2O_2 are scavenged
6 completely by clouds, ii.) $\gamma_{\text{N}_2\text{O}_5} = 0.01$ and iii.) HNO_3 is not scavenged by aerosols (or
7 rain) following injection into the UT.

8

9 **2.1 Treatment of OH and HO₂**

10 The calculated time since convective detrainment is directly coupled to the HO_x budget
11 through the daytime NO_x sink to HNO_3 via reaction with OH. As in other model
12 descriptions of the UT during INTEX-NA (2, 3), our unconstrained model over-estimates
13 OH by nearly a factor of two in the UT and under-estimates HO_2 by a similar amount.
14 Due to the direct dependence of our timing indicator on HO_x , we constrain the mixing
15 ratios of OH and HO_2 to the observed values as a function of NO_x and altitude. Figure
16 S3 depicts the modeled mixing ratios of OH and HO_2 (lines), constrained to the
17 observations (dots), as a function of NO_x and SZA at 10km. The observed OH is a strong
18 function of NO_x , while observations of HO_2 remain insensitive to NO_x . Constraints for
19 OH and HO_2 were derived independently for each 1km altitude bin. Constraining OH
20 and HO_2 to the observations increases the time required for the NO_x - HNO_3 system to
21 reach steady-state (by slowing the rate of $\text{OH} + \text{NO}_2$) and enhances the modeled O_3
22 production in the outflow region (by speeding up the rate of $\text{HO}_2 + \text{NO}$).

23

1 **2.2 Calculation of Time since Convection**

2 The time since a sampled air-mass had been cloud processed is calculated by applying the
3 mapping of time to NO_x/HNO_3 derived in the box model to the observed NO_x to HNO_3
4 ratio. Figure S4 depicts the best-fit relation between the modeled NO_x to HNO_3 ratio and
5 time since cloud processing at 10km. This function is calculated at 1km increments from
6 6-12km and applied to the measured NO_x to HNO_3 ratio. In this analysis we calculate
7 NO_x from observations of NO_2 , O_3 , HO_2 and photolysis rates measured directly on the
8 DC-8. We use the Cal-Tech CIMS HNO_3 due to its fast time response (5 seconds as
9 compared to 105 seconds for the UNH Mist Chamber Technique) and the UNH MC
10 results when the fast HNO_3 was unavailable. To account for the systematic bias between
11 the two observations in the UT ($[\text{HNO}_3]_{\text{UNH}} = 0.6 \times [\text{HNO}_3]_{\text{Cal-Tech}}$), we scale both the
12 CIMS and MC observations to split the difference between the two measurements (i.e.
13 we increase $[\text{HNO}_3]_{\text{UNH}}$ by 20% and decrease $[\text{HNO}_3]_{\text{CIT}}$ by 20%).

14

15 **2.3 Model Assumptions and Uncertainty**

16 In order to access the uncertainty in the calculated time, we ran the time-dependent model
17 under various different conditions encountered during INTEX-NA (e.g. $[\text{NO}_x]_i$ (0.2-3.0
18 ppbv), $[\text{O}_3]_i$ (40-100 ppbv), $[\text{CO}]_i$ (80-150 ppbv), detrainment time (noon, 4PM,
19 midnight), altitude (6-12km) and time of year (June-September). As illustrated in figure
20 S4, the NO_x to HNO_3 ratio has good resolution (i.e. large rate of change per unit time)
21 during the first five days following convection. Beyond five days small changes in
22 NO_x/HNO_3 correspond to larger changes in the derived time. From the variance in the
23 calculated time of individual model runs, we estimate the uncertainty in our modeled time

1 to be ± 6 hours at 1 day, ± 12 hours at 2 days and ± 1 day at 4 days. In addition, the
2 INTEX-NA sampling domain did not permit frequent measurement of aged convection
3 (>5 days). For these reasons we limit our analysis to the first five days following
4 convection.

5

6 **2.4 Treatment of Mixing**

7 To access the effects of mixing on the chemistry occurring in the outflow region, we look
8 at the evolution of long lived species as a function of our calculated time since
9 convection. The dilution rate was determined by iterating the model until we had closure
10 between the observed and modeled time evolution of a suite of long-lived species (e.g.
11 CH_4 , CO_2 and CH_3OH). We find this mixing term to be $0.05 \pm 0.02 \text{ day}^{-1}$. This rate
12 supports the conclusion that over the course of 5 days, the convective plume remains
13 relatively isolated from the background UT. Due to subsidence of convectively lofted
14 air parcels following injection, our calculated time represents a lower bound for age as
15 the chemical clock speeds up (due to NO_x repartitioning) as the parcel descends in
16 altitude. However, this is a relatively small effect as calculated subsidence rates are
17 approximately 200m day^{-1} .

18

19 **3.0 Comparison of Chemical and Meteorological Convective Influence Calculations**

20 The results presented here provide a chemical constraint on the rate at which the UT over
21 the continental US is influenced by convection during summer. Fuelberg et al. conducted
22 an independent meteorological evaluation of the influence of convection during the
23 INTEX-NA field campaign using kinematic back trajectories coupled with National

1 Weather Service's Global Forecast System (GFS) derived convection (4). In their
2 analysis they find that the DC-8 sampled air influenced by convection within the last two
3 days 63% of the time (compared to 54% in this analysis). Figure S5 illustrates the
4 strong agreement between the two independent techniques. Further, the meteorological
5 analysis can be used to test how representative the sampling during the INTEX-NA
6 experiment was of the continental summer UT. Fuelberg et al. conclude that the DC-8
7 sampled air that was influenced by convection within the past 6 hours 21.4% of the time.
8 Applying the GFS analysis to the entire INTEX-NA domain, they concluded that the
9 continental US during summer was influenced by convectively influenced air less than 6
10 hours old 12.5% of the time, suggesting that the DC-8 had a positive bias toward
11 sampling fresh convection.

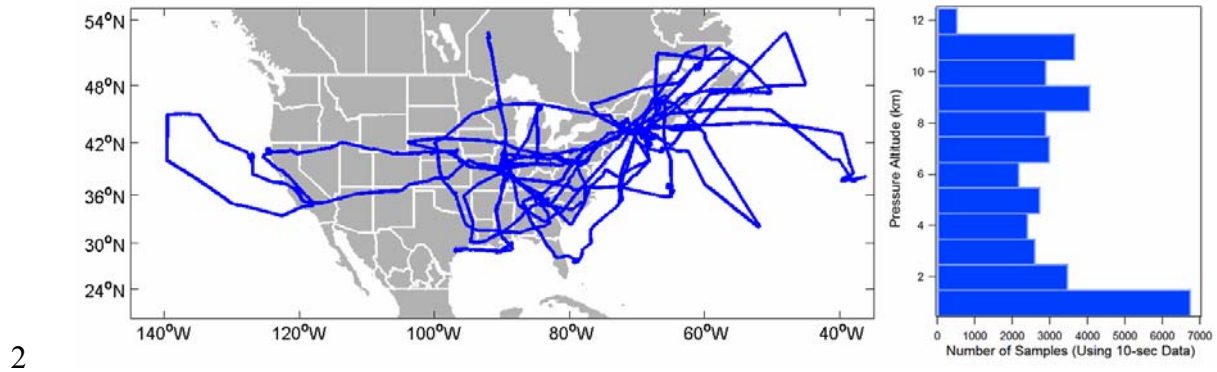
12

13 **4.0 Current Assessment of Convective Parameterization in Global Models**

14 Due to the coarse resolution of global models (100-1000km), sub grid scale processes
15 such as convection necessitate parameterization (5, 6). The treatment of convection in
16 these models is usually assessed through comparison of the model with measured vertical
17 distributions of ^{222}Rn (a terrestrial tracer with a 5 day e-folding time to radioactive decay)
18 over the continents and of methyl iodide (a oceanic tracer with a 4-day e-folding time to
19 photolysis) over the ocean (5, 7-10). This assessment technique is dependent on the
20 accuracy of the modeled surface ^{222}Rn source distribution and is hindered by a limited
21 number of vertical profiles available to directly constrain convective mass fluxes and the
22 resulting rate at which air in the upper troposphere is turned over. Of the 23 summer-
23 time continental profiles in ^{222}Rn compiled by Liu et al., only 6 contain measurements

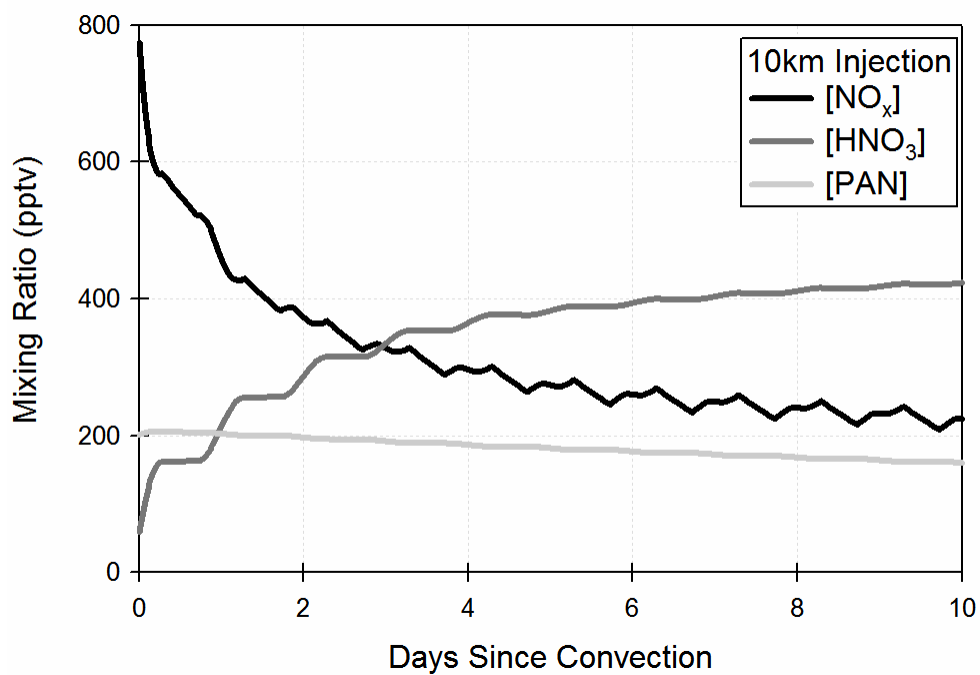
1 above 7.5 km and only 2 above 9 km (11). Beyond the Liu et al. compilation, we are
2 aware of only two other studies of the tropospheric vertical distribution of ^{222}Rn (Zauker
3 et al. (12) made observations of ^{222}Rn up to 6km over Nova Scotia in August of 1993 and
4 Kritz et al. (13) made measurements to 11.5km on 11 research flights during the summer
5 of 1994 over San Francisco, CA). For comparison, our observations include 52 en-route
6 or orbit profiles, more than doubling the size of the existing UT ^{222}Rn data set and
7 providing much higher resolution.

8

1 **2. Supplemental Figures**

3 **Figure S1:** *left panel* INTEX-NA flight tracks made between 1 July 2004 and 14 August
4 2004 aboard the NASA DC-8. *right panel* Number of samples (using 10-sec averaged
5 data) within 1 km altitude bins between 0-12 km during the entire campaign.

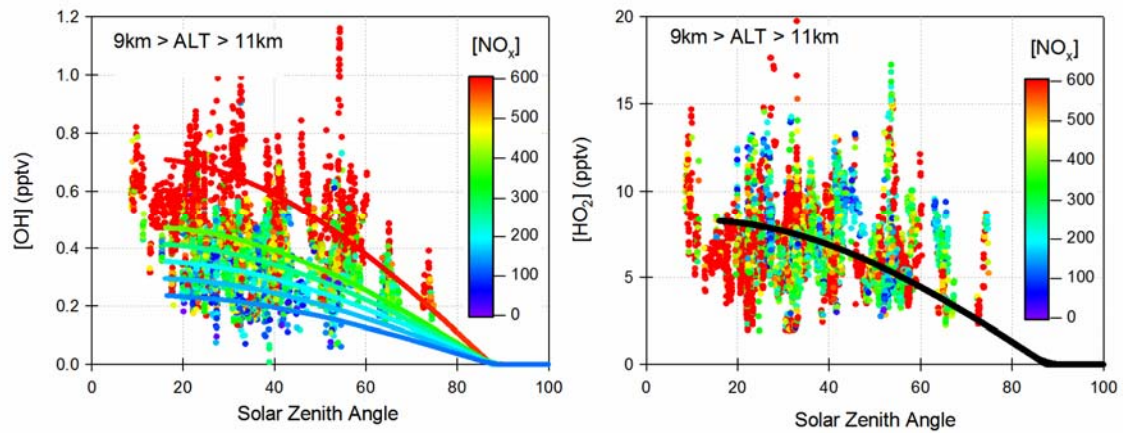
1



2

3 **Figure S2:** Time-dependent model illustrating the conversion of NO_x to Nitric Acid in
4 the days subsequent to a cloud processing event occurring at 10km. The above model
5 was initialized at 12PM local time at 30°N in August using [NO_x]_i = 800 pptv, [CO]_i =
6 105 ppbv at [O₃]_i = 65 ppbv.

1

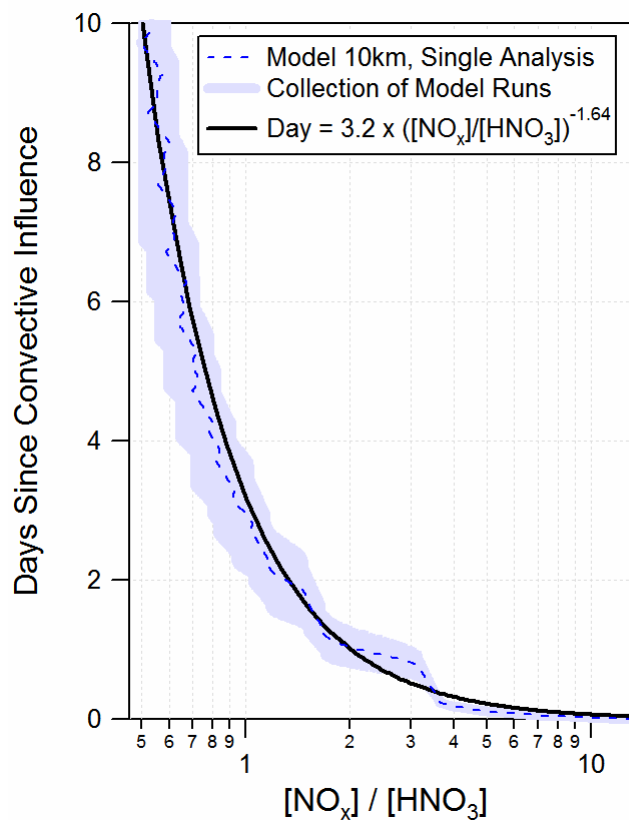


2

3

4 **Figure S3:** Model representation of OH (left panel) and HO₂ (right panel) as a function
5 of SZA and [NO_x]. Model results (solid lines) are shown on top of the *in situ*
6 observations (dots). The model was initialized at noon at 10km with [NO_x]_i = 800 pptv,
7 [CO]_i = 105 ppbv at [O₃]_i = 65 ppbv. Observations shown were taken aboard the DC-8
8 between 9 and 11 km.

1

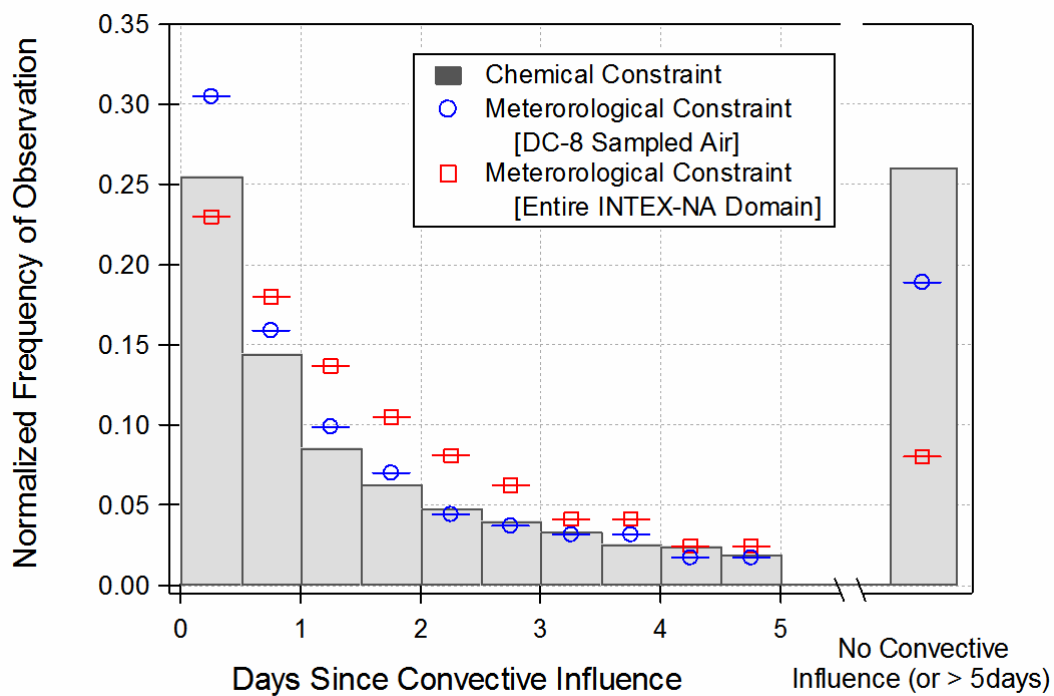


2

3

4

5 **Figure S4:** Observed NO_x to HNO₃ ratios are converted to a time since last convective
6 influence using the best fit equation relating the NO_x/HNO₃ ratio to time as calculated
7 using the time-dependent model in 1km altitude bins from 7.5-11.5 km. The above
8 equation is valid for pressure altitudes between 9.5 and 10.5 km.



1
2
3
4
5
6

Figure S5: Comparison of chemical (grey bars) and meteorological constraints (-○-, -□-) on convective influence during INTEX-NA. Convective influence on air *sampled* by the DC-8 is shown with blue circles (-○-), while convective influence on the entire INTEX-NA domain is shown with red squares (-□-).

1

Species	Measurement Technique	Detection Threshold	Accuracy	Time Response	Reference
NO ₂	LIF ¹	8 pptv / 10 sec	±10% 1σ	1 Hz	(14, 15)
HNO ₃	CIMS ³				
	Mist Chamber – IC ⁴	5 pptv / 105 sec		105 sec	(16)
OH	LIF ¹	0.01 pptv	±32% 2σ - 1 min	20 sec	(17)
O ₃				1 Hz	(18)
CO	IR-Absorption	Precision = ±1ppbv, ±1.5% of reading	±1.4 ppbv, ±2.6% 2σ	1 Hz	(19)
CO ₂	IR-Absorption	Precision < 0.07 ppmv		1 Hz	(20)
SO ₂	CIMS ³			1 Hz	
UCN	TSI CN counter ⁵			1 Hz	

2

¹LIF – Laser Induced Fluorescence

3

NO₂ detection threshold is 8 pptv / 10 sec at 760 Torr (ground) and 20 pptv / 10 sec at 200 Torr (10 km)

4

³CIMS – Chemical Ionization Mass Spectrometry

5

⁴IC – Ion Chromatography

6

⁵UCN (Ultra-fine Condensation Nuclei) was obtained by the difference of the UCN (D_p>3nm, TSI 3025) and CN (D_p>10nm, TSI 3010) Condensation Nuclei (CN) instruments.

7

8

9

Table S1: Detection thresholds, measurement uncertainty and time response of the *in situ* measurements used in this study.

10

References:

1. H. B. Singh, W. H. Brune, J. H. Crawford, D. J. Jacob, *Submitted Journal of Geophysical Research - Atmospheres* (2006).
2. X. R. Ren *et al.*, *Submitted Journal of Geophysical Research - Atmospheres* (2006).
3. R. C. Hudman *et al.*, *Submitted Journal of Geophysical Research - Atmospheres* (2006).
4. H. E. Fuelberg, M. J. Porter, C. M. Kiley, D. Morse, *Submitted Journal of Geophysical Research - Atmospheres* (2006).
5. D. J. Jacob *et al.*, *Journal of Geophysical Research-Atmospheres* **102**, 5953 (Mar 20, 1997).
6. D. J. Allen, R. B. Rood, A. M. Thompson, R. D. Hudson, *Journal of Geophysical Research-Atmospheres* **101**, 6871 (Mar 20, 1996).
7. D. J. Jacob, M. J. Prather, *Tellus* **42B**, 118 (1990).
8. D. Rind, J. Lerner, *Journal of Geophysical Research-Atmospheres* **101**, 12667 (May 20, 1996).
9. W. J. Collins, R. G. Derwent, C. E. Johnson, D. S. Stevenson, *Q.J.R. Meteorol. Soc.* **128**, 991 (2002).
10. N. Bell *et al.*, *Journal of Geophysical Research-Atmospheres* **107** (Sep, 2002).
11. S. C. Liu, J. R. McAfee, R. J. Cicerone, *Journal of Geophysical Research-Atmospheres* **89**, 7291 (1984).
12. F. Zaucker *et al.*, *Journal of Geophysical Research-Atmospheres* **101**, 29149 (Dec 20, 1996).
13. M. A. Kritz, S. W. Rosner, D. Z. Stockwell, *Journal of Geophysical Research-Atmospheres* **103**, 8425 (Apr 20, 1998).
14. J. A. Thornton, P. J. Wooldridge, R. C. Cohen, *Analytical Chemistry* **72**, 528 (Feb 1, 2000).
15. P. A. Cleary, P. J. Wooldridge, R. C. Cohen, *Applied Optics* **41**, 6950 (Nov 20, 2002).
16. R. W. Talbot *et al.*, *Journal of Geophysical Research-Atmospheres* **102**, 28303 (Dec 20, 1997).
17. I. C. Faloona *et al.*, *Journal of Atmospheric Chemistry* **47**, 139 (Feb, 2004).
18. M. A. Avery, *Submitted Journal of Oceanic and Atmospheric Technology* (2006).
19. G. W. Sachse, G. F. Hill, L. O. Wade, M. G. Perry, *Journal of Geophysical Research* **92**, 2071 (1987).
20. B. E. Anderson *et al.*, *Journal of Geophysical Research-Atmospheres* **101**, 1985 (Jan 20, 1996).

Co-author comments on “*Chemical constraints on convective influence*”

Comments #1-----

1.) How did you treat the HNO₃ measurement bias in the UT. It seems your basic story would not change, but the numeric values would, if you used lower HNO₃ values in much of the UT. Seems this would lead to even greater convective influence and faster turnover.

- We have run the analysis using all possible combinations of measurement techniques for both NO_x and HNO₃. The bottom-line is that the story stays the same, but the numbers change (e.g. ~10-20% more convection if using UNH HNO₃ compared to Cal-Tech HNO₃). Tables 1 & 2 below illustrate the effects of using various combinations of measurement techniques on the calculated fraction of UT air that was influenced by convection during the past two days. The numbers used in this analysis are shown in red.

We have chosen to calculate NO_x from NO₂, O₃, HO₂ and photolysis rates, assuming NO-NO₂ to be in steady-state. We prefer to avoid a lengthy discussion of sampling biases in this manuscript, so we have scaled both the Cal-Tech and UNH HNO₃ numbers to split the difference of the apparent bias (Figure 1). Since the convective plumes that we sampled appear to be ~200 seconds wide in the horizontal (40 km @ 200 m/sec) FWHM, but less than a km thick in the vertical, we chose to using the (scaled) Cal-Tech HNO₃ and UCB NO₂ in this analysis due to their fast time response.

2.) page 8, full para in middle instead of "The figure confirms" I would say "Figure 4 d confirms" since it is a while since you called out any fig (and it was 4a)

-Done

3.) page 9 I find the discussion of the CO₂ filter on CO a bit terse. What is magic about 376 ppm CO₂? Also, in the last sentence you send the reader to Fig 1 to verify that CO₂ is a good BL tracer, but there is no CO₂ in this figure. Should this be Fig 3?

-Agreed, our hope was to look at the time evolution of CO on a constant CH₄ isopleth (c.f. Figure 2). Unfortunately, since we do not have fast CH₄ from INTEX it was hard to find a surrogate long lived species that was sampled fast enough to do this analysis. Due to the strong anti-correlation of CO and CO₂ in the UT during INTEX-NA, we chose an arbitrary CO₂ band (CO₂ < 376 ppmv) to look at CO decay in the first draft. We have dropped this constraint in this version, opting to take on the added atmospheric variance in the figure.

4.) page 10 top "The source of the discrepancy.."

-Done

5.) last full para "with the observed O3 ppbv" seems you are missing a numeric value after O3

-Done "with the observed O₃ 15 ppbv "

6.) p11, bottom "However, there is a very limited.."

-Done

7.) p12, top Did Kritz never publish more Rn profiles? I thought he measured them on space available basis on Kuiper flights for some years.

- Kritz et al. 1998 is the only record I can find of his "piggy-back" measurements made on the Kuiper. It appears that he made them on numerous flights, but we could not find any record of this in the literature. I will include them if we find any. Our point here was that global models are constrained by a limited set of Rn profiles (the ones referenced here). If there are more available it doesn't seem like the modeling community has taken advantage of them. The ²²²Rn discussion has been moved to the supplement due to space limitations

8.) in the caption for Fig 5 it is not clear to me how you were able to calculate 24 hour average OH from the observations. Presumably this is a hybrid of model and observations, but as stated it seems someone measured OH from the DC-8 in the UT around the clock

-Yes, this is a hybrid product. I have scaled the instantaneous OH to 24-hour OH as a function of SZA. Since we ended up constraining our model to the observed OH and HO₂, the OH vs. time did not have great significance. It has been removed. The supplement as two figures OH and HO₂ vs SZA and NO_x that describe our representation of HO_x in the time dependent model.

Comments #2 -----

1.) I think that the ozone results are very interesting - along these lines even though you are pressed for space - you might give some more detail about ozone prod/loss i.e. state if you are using calculated or measured HO₂ and give some idea of the loss terms. i.e. HO₂+O₃, etc.

-Agreed. We have attempted to do this in the supplemental information. If we end up sending to JGR, this will become a more detailed part of the paper (along with an in depth discussion of uncertainties). We understand that there is a large discrepancy between the modeled and observed OH and HO₂ in the UT. This affects us in two ways: i.) the speed of our clock is directly coupled to HO_x through OH+NO₂ and ii.) our O₃

production is driven by $\text{NO} + \text{HO}_2$. For this reason we have constrained our model to the observed OH and HO_2 as a function of altitude and NO_x (see supplemental information).

2.) I am a little lost on how you know the overturning rate on the air from the NO_x/HNO_3 clock, i.e. how do you take out the effect of lightning NO_x injected into the convecting air parcels. I may be missing this argument as I looked at it quickly.

*-Since we are looking at the ratio of NO_x/HNO_3 as an indicator of time since convection, we are relatively insensitive (to the extent to which it perturbs the HO_x budget) to the magnitude of NO_x that is injected into the UT. If lightning NO_x is added to the convective outflow it should have no effect on our ability to track time and calculate an over-turn rate. However, if lightning occurs **without** convection (without cloud-processing), then we will over estimate the over-turn rate as we would mark that air-mass as being convectively influenced. Basically our clock is initialized by any event that re-sets the NO_x/HNO_3 ratio. The time evolution of UCN and HNO_3 support that that event is convection / cloud processing.*

Comments #3-----

1.) Abstract:

Here and at least one other place in the paper you mention measurements of NO_x yet you also mention in the paper that the observations consisted of NO_2 , etc (page 4) with never a mention of NO measurements. I presume you use the Brune NO data. If so then be sure to state so with some reference to the instrument performance.

-In this analysis we calculate NO_x from our observations of NO_2 assuming $\text{NO}-\text{NO}_2$ is in steady-state. This has been clarified in the text and in the supplemental information.

2.) Figure 3 caption:

Typo “in shown in Panel D” should be “is** shown in Panel D.”**

-Done

It’s almost impossible to see the back trajectory.

-We have added a black edge color to the trajectory dots to make them stand out more clearly.

3.) Figure 5 caption:

The conditions $[\text{CO}_2] < 376$ ppm and altitude > 8 km are said to apply to the CO and OH Panels but there is no mention if these constraints apply to the O3 Panel. If it doesn’t apply, then make it more clear otherwise there may be some uncertainty to the reader.

-Agreed. We have further clarified when/where we have applied constraints in the text. As for the CO₂ constraint, it was removed completely (as mentioned previously).

4.) I'm having a problem understanding the assumption that you look at a "chemically isolated lamina" to look at its chemical evolution yet a conclusion of the paper is that the UT is turning over much more rapidly than others have concluded. Then how can the "Days Since Cloud Processing" go out to 5 days in figure 5? The "chemically isolated lamina" assumption should have fallen apart well before then. What happens if you have a CO₂ panel in figure 5? If the CO₂ mean stays relatively constant it verifies the "chemically isolated lamina" assumption over some number of days. If it drops quickly it verifies the rapid turning over of the UT. Would looking at CO₂ with respect to "Days Since Cloud Processing" or in some other way help verify the mean turn over time of the UT?

-This is one of the areas that we have changed considerably since the previous version in a number of different ways. 1.) Since we have constrained our model to the observed OH and HO₂, we can use the decay in CO and other long-lived species to calculate entrainment of background air into the convective plume. In this analysis (page 9) we determine from CO, CH₄, CH₃OH and others that plume entrains air from the background UT at 5% per-day (which is quite slow). We show the modeled and observed time evolution of CH₄, CO₂ and CH₃OH in the figure included below. 2.) To calculate the turnover rate of the UT, we have used our frequency distributions coupled with our calculation of the fraction of BL air found in fresh convection. We show that using a simple model that you expect to see a small fraction of air that about 5 days old assuming an overturn rate of 10-20% day. When looking at the frequency distribution presented in figure 6b, you can see that there is relatively little sampled air that had been influenced by convection between days 3-5. This is largely because air that was convected within our sampling window is for the most part well east of the DC-8 reach by days 3-5. In contrast there is a significant fraction of very old air (or stratospheric air) >25%. We have tried to explain these effects using a simple model described on page 14.

Comments #4-----

1.) P6. You might want to mention why the air is depleted in CO₂ by including something akin to "Sharp decreases in CO₂ also indicate the convective lofting of boundary layer air depleted in CO₂ from the seasonal photosynthetic activity in the biosphere."

-Done

2.) P9. CO₂ was chosen as an appropriate filter due to its relatively long lifetime,...(as seen in figure. Suggest including relatively as the lifetime can vary from hours to 150 years.

-We have actually decided to remove the CO₂ filter on these figures(see previous discussion)

3.) Figure 3. Would it be possible to use black as an edge color on the trajectory symbols so they would be more visible to the viewer?

-Done

4.) It may be worth mentioning how the summer of 2004 fits into the climatological scheme of things i.e. was this was an average summer or anomalous in terms of storms, ENSO cycle, weather patterns. Recall Ann Thompson's ICARTT presentation being titled "The summer that wasn't".

-Agreed. We have included a short section in the supplement that targets how representative our sampling was of the continental UT during summer. We are also working on a comparison to the modeled convective mass fluxes with Ken Pickering.

5.) In the abstract and on page 3, UT O₃ and its impact on climate are mentioned. Can you extrapolate your findings i.e. does the radiative forcing of 0.4 to 0.78 W m⁻² given on page 3 change as a result of this study?

-I wish that we could, but we feel that it would be over-stepping the abilities of this analysis. It is unclear whether the UT O₃ column is enhanced or suppressed as a result of convection, as the fast O₃ production is balanced by convective lofting of boundary layer air depleted in O₃. This should however be a focus of a larger modeling study.

6.) There is a paper that may be of interest by G. L. Mullendore et al., Cross-tropopause tracer transport in midlatitude convection, JGR, 116(D06113, doi:10.1029/2004JD005059, 2005 that quantifies the mass transport from the lower troposphere to the UT and LS via extratropical convective storms. Recalling mention of multi-cell storms having updrafts in the core of up to 50 – 60 ms⁻¹.

-Great, I have included this to strengthen the argument of strong local influence from supercell and multicell storms

Comments #5-----

1.) How did you treat the inconsistency between HNO₃ measurements in the UT and the noisy NO numbers in the mid-troposphere.

-Please see the above comments to co-author #1

2.) How much resolution do you have in the model at long-time? Does this significantly affect your assessment of O₃ production past 2-3 days?

We feel we have good resolution in the model out to 5 days (c.f. supplemental figure S4). However, we simply did not sample air that was 3-5 days old very often during INTEX. Thus, it is true that it is more difficult to quantify the chemistry occurring past 3 days and we should be careful not to make any strong conclusions based upon days 3-5. We have added this to the list of possible explanations for the missing L_{Ozone} .

3.) General statistics question: Use quartiles instead of standard deviations. Does using means vs. medians affect the results significantly?

-The 1st and 3rd quartiles have been included in all of the figures. Means and medians are also included on each figure.

Comments #6-----

1.) As there is a lot of scatter from Figures 2 and 4, we should somehow state the degree of confidence any single measurement ratio tells us the age. I believe that you have further averaged things into 10-second bins. What do things look like then? I am afraid that a reviewer will see the large scatter and will question the ability to tell air mass age since convection. We should state something to the effect that despite this scatter, on average (or something to this effect) the NO_x/HNO_3 ratio provides this information.

This is an important point as the scatter does not reflect error in the ability to mark time, but reflects the natural atmospheric variability. We expect the initial chemical composition of each convective plume to be quite different, thus driving a wide spread in species vs. time. This is shown nicely in figure 2 (below) where we plot CO vs. time on a constant CH_4 isopleth. Additionally the chemical evolution of plumes at different altitudes should be quite different due to varying HO_x etc. All of the figures here are made with the 10-second data merge. I tried doing the analysis at a constant altitude and basically on any isopleth I could imagine. Unfortunately, further binning of the data simply decreases the number of samples, making any conclusions a bit tricky. In the current version I have used a shaded region to represent the 1st-3rd quartiles and included the model results and the medians. I think this helps draw the reader's attention toward the agreement (or disagreement) between the model and measurement. I have also included a short discussion on assumptions and uncertainty in the derivation of time in the supplemental information.

2.) By the way, does Fig 2 show the mean values by the points and the solid line?

- Yes, the points and lines represent the mean value within the altitude bin, this has been clarified in the figure caption.

3.) Page 10: 2nd para regarding the lower O_3 in convectively lofted air calculated compared to observations: what about $\text{HO}_2 + \text{O}_3$ and $\text{OH} + \text{O}_3$ loss terms. I know you mention this later on, but can extra HO_x be responsible for this discrepancy?

We include OH and HO₂ + O₃ in the model. In the current version we have constrained the model to the observed OH and HO₂ to avoid these problems. However, if we have an error in HO_x, we will have problems in a series of loss (and production) terms, in addition to the speed of our chemical clock (due to NO₂+OH). I think we should also be careful of drawing strong conclusions on data from 3-5 days, due to the error in our derived time and the limited sample size at these times (c.f. figure 6 of the paper)

4.) Page 6, right after the references (20,21,23-27) add a comma.

-Done

A. Effects of HNO₃ Measurement (Cal-Tech CIMS vs. UNH Mist Chamber)

Altitude	Case 1	Case 2	Case 3	Case 4	Case 5	Case 6
7.5 – 8.5 km	0.45	0.39	0.42	0.44	0.34	0.43
8.5 – 9.5 km	0.64	0.50	0.54	0.64	0.47	0.56
9.5 – 10.5 km	0.77	0.61	0.67	0.77	0.61	0.69
10.5 – 11.5 km	0.59	0.23	0.44	0.59	0.32	0.43
Entire UT (Altitude >7.5 km)	0.62	0.47	0.53	0.63	0.45	0.54

Case 1: HNO₃ from UNH MCCase 2: HNO₃ from CIT CIMSCase 3: HNO₃ from CIT CIMS + UNH MCCase 4: HNO₃ from CIT CIMS (Scaled to UNH) + UNH MCCase 5: HNO₃ from CIT CIMS + UNH MC (Both Scaled to Difference)Case 6: HNO₃ from CIT CIMS + UNH MC (Both Scaled to Difference)*NO_x calculated from UCB NO₂

Table 1: Effects of NO_x measurement technique on the fraction of air that had been cloud processed during the past two days

B. Effects of NO_x Measurement (UCB NO₂ vs. Penn-State NO)

Fraction of air that had been cloud processed during the past two days

Altitude	Case 1	Case 2	Case 3
7.5 – 8.5 km	0.39	0.52	0.53
8.5 – 9.5 km	0.50	0.66	0.68
9.5 – 10.5 km	0.61	0.64	0.70
10.5 – 11.5 km	0.23	0.30	0.32
Entire UT (Altitude >7.5 km)	0.47	0.58	0.61

Case 1: NO_x calculated from UCB NO₂Case 2: NO_x calculated from PS NOCase 3: NO_x calculated from UCB NO₂ + PS NO*HNO₃ from Cal-Tech CIMS

Table 2: Effects of HNO₃ measurement technique on the fraction of air that had been cloud processed during the past two days

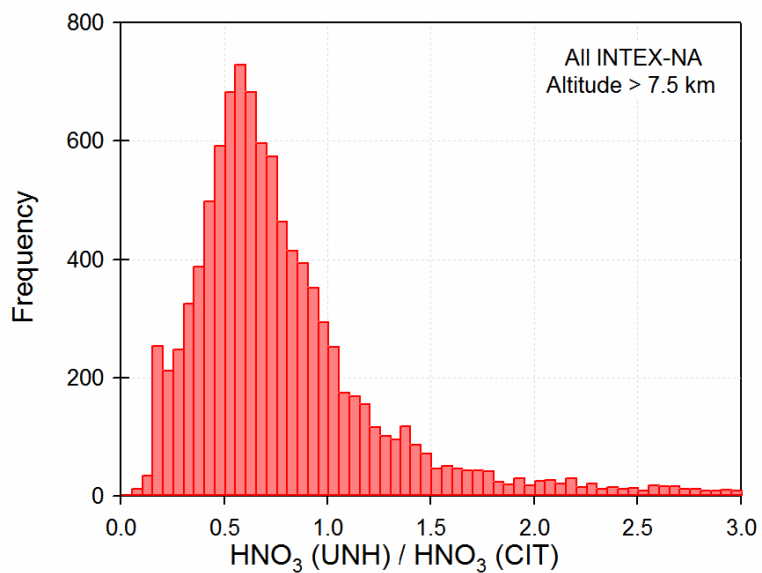


Figure 1: Sampling bias between Cal-Tech and UNH HNO_3 Observations in the UT (Altitude>7.5km).

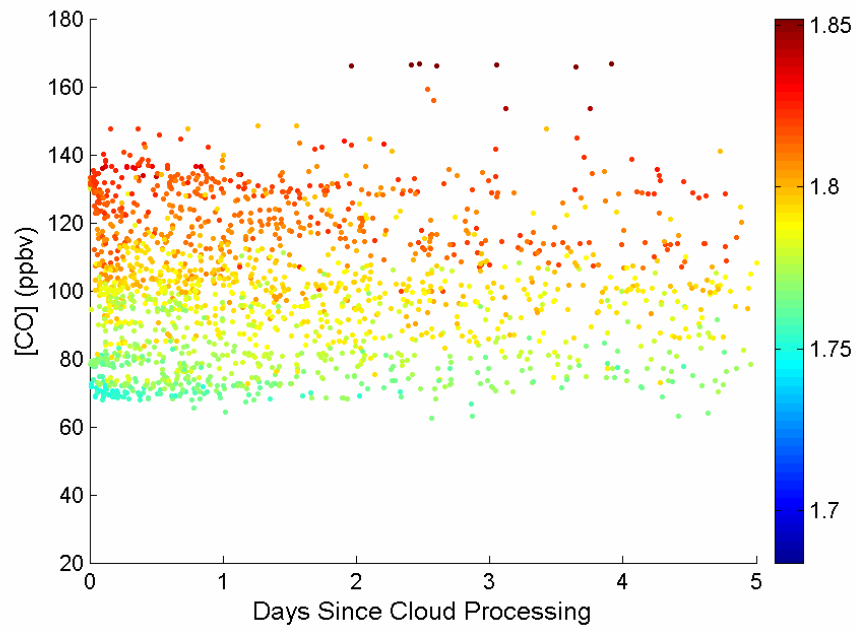


Figure 2: Observations of CO as a function of modeled time since convective influence in the UT. CO observations are color-coded by methane.

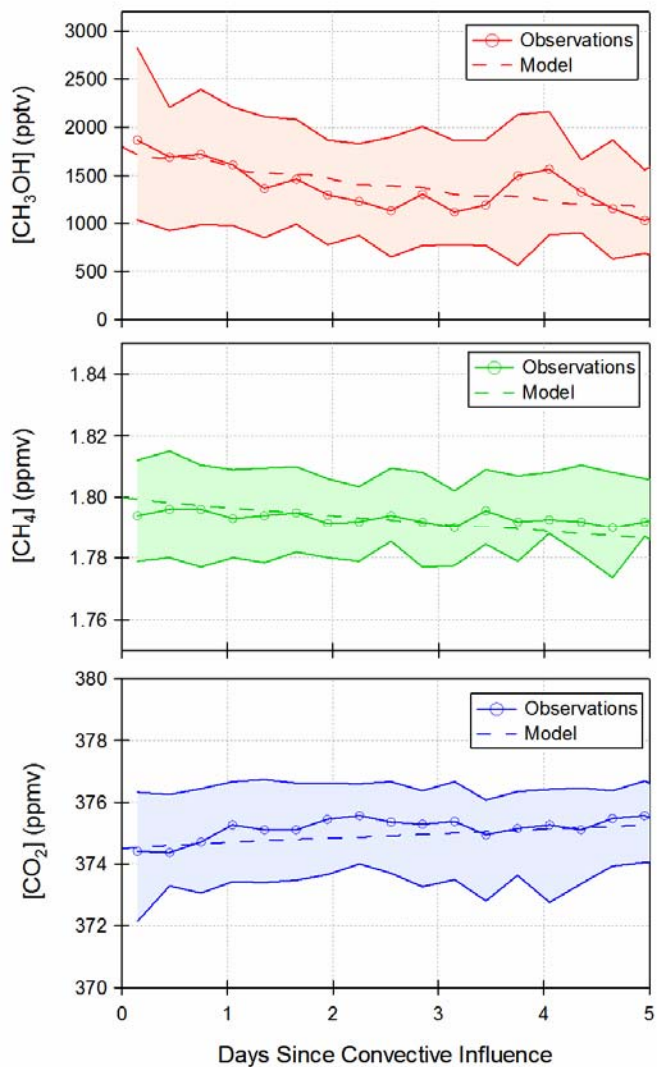


Figure 3: Observations of Methanol (CH₃OH), Methane (CH₄) and CO₂ as a function of modeled time since convective influence. The median (-○-) of the observations, within 8 hour bins, is shown along with the 1st and 3rd quartiles (shaded region). Results from the time-dependent box model, initialized at 10 km and 12PM, are shown with dashed lines.